Micron 43 (2012) 1331–1335

Contents lists available at SciVerse ScienceDirect

Micron

journal homepage: www.elsevier.com/locate/micron

Magnetosomes and magnetite crystals produced by magnetotactic bacteria as resolved by atomic force microscopy and transmission electron microscopy

Zachery Oestreicher[a], Carmen Valverde-Tercedor[b], Lijun Chen[a], Concepcion Jimenez-Lopez[b], Dennis A. Bazylinski[c], Nadia N. Casillas-Ituarte[a], Steven K. Lower[a], Brian H. Lower[a,*]

[a] The Ohio State University, 210 Kottman Hall, Columbus, OH 43210, USA
[b] Universidad de Granada, Departamento de Microbiologia, Campus de Fuentenueva, 18071 Granada, Spain
[c] University of Nevada, Las Vegas, School of Life Sciences, 4505 South Maryland Parkway, Las Vegas, NV 89154, USA

ARTICLE INFO

Article history:
Received 31 December 2011
Received in revised form 4 April 2012
Accepted 4 April 2012

Keywords:
AFM
Biomineralization
Magnetite
Microorganism
TEM

ABSTRACT

Atomic force microscopy (AFM) was used in concert with transmission electron microscopy (TEM) to image magnetotactic bacteria (*Magnetospirillum gryphiswaldense* MSR-1 and *Magnetospirillum magneticum* AMB-1), magnetosomes, and purified Mms6 proteins. Mms6 is a protein that is associated with magnetosomes in *M. magneticum* AMB-1 and is believed to control the synthesis of magnetite (Fe_3O_4) within the magnetosome. We demonstrated how AFM can be used to capture high-resolution images of live bacteria and achieved nanometer resolution when imaging Mms6 protein molecules on magnetite. We used AFM to acquire simultaneous topography and amplitude images of cells that were combined to provide a three-dimensional reconstructed image of *M. gryphiswaldense* MSR-1. TEM was used in combination with AFM to image *M. gryphiswaldense* MSR-1 and magnetite-containing magnetosomes that were isolated from the bacteria. AFM provided information, such as size, location and morphology, which was complementary to the TEM images.

1. Introduction

Environmental microbiologists are often interested in understanding the molecular-scale biogeochemical reactions that occur between a biomolecule, such as a protein, and a mineral surface. For example, microbial proteins can catalyze the synthesis of mineral phases by influencing crystal nucleation and/or growth (Bazylinski and Frankel, 2004; Hernández-Hernández et al., 2008). These reactions in turn control the bioavailability of elements to the surrounding ecosystem, which can have profound affects (both positive and negative) on water quality, mineral distribution, migration of subsurface contaminants, and soil productivity (Barton and Fauque, 2009; Dittrich and Luttge, 2008; Edwards et al., 2005; Hochella et al., 2008; Madsen, 2011; Weber et al., 2006).

It is a challenge to probe reactions that occur between a microorganism (or protein) and mineral due to the small size of the reacting space as well as the fact that the interface itself is hidden from direct view. Transmission electron microscopy (TEM) affords the spatial resolution and, with the aid of a diamond microtome, the ability to visualize the interface. But, TEM operates in a vacuum rendering cells dead and biomolecules in a "non-hydrated" state. Atomic force microscopy (AFM) allows one to image living cells in solution so that biomolecules are in their naive state. While, AFM is capable of atomic resolution, it can be challenging to achieve high resolution with soft, deformable samples like cells. In this paper, we compare and contrast TEM and AFM analyses of proteins and minerals produced by two magnetotactic bacteria: *Magnetospirillum gryphiswaldense* MSR-1 and *Magnetospirillum magneticum* AMB-1.

These two magnetotactic bacteria use specific proteins (e.g., Mms6) to synthesize magnetite (Fe_3O_4) nanoparticles within a membrane-bound organelle called a magnetosome (Bazylinski and Frankel, 2004). Each bacterium contains up to 60 magnetosomes and each magnetosome contains one magnetic Fe_3O_4 nanoparticle (Bazylinski and Frankel, 2004). The magnetosomes are aligned in a chain-like fashion, which imparts a magnetic dipole to the bacterial cell, allowing the cell to align itself within Earth's geomagnetic field (Bazylinski and Frankel, 2004). In addition, magnetotactic bacteria have a flagellum, which they use for mobility.

We demonstrate that AFM can be used to obtain high-resolution images of subcellular structures synthesized by a living *M. gryphiswaldense* MSR-1 bacterium. We show complementary TEM and AFM images of magnetosomes isolated from *M. gryphiswaldense* MSR-1. We also collected AFM images of individual Mms6 proteins on magnetite immersed in solution. We chose to image Mms6 because it is a magnetosome-associated protein from *M. magneticum* AMB-1 that has been implicated in mediating the

* Corresponding author. Tel.: +1 614 247 1676; fax: +1 614 292 7432.
E-mail address: Lower.30@osu.edu (B.H. Lower).

0968-4328/$ – see front matter © 2012 Elsevier Ltd. All rights reserved.
http://dx.doi.org/10.1016/j.micron.2012.04.002

synthesis of magnetite in these bacteria (Bazylinski and Frankel, 2004).

In general, the TEM provides higher resolution of ultrafine features, but the AFM reveals the association of proteins and minerals in their natural environment where protein expression and location are regulated, and where molecular neighbors can influence function. In this way, AFM confirms that TEM records the native structural relationship of proteins and minerals with living cells, for properly prepared specimens. Ongoing experiments are aimed at using AFM to observe real-time growth of magnetite in the presence of Mms proteins.

2. Materials and methods

2.1. Growth and preparation of bacteria for AFM and TEM

Small cultures (e.g., 50–100 mL) of the magnetotactic bacterium *M. gryphiswaldense* MSR-1 were grown in flask standard medium under microaerobic conditions (100 rpm) at room temperature (Heyen and Schuler, 2003). Because these microbes synthesize magnetite (Fe_3O_4) nanoparticles, simple bar magnets were used to isolate and concentrate the *M. gryphiswaldense* MSR-1 from the cultures after several days of growth. The concentrated bacterial samples were then spotted onto a carbon coated 200 mesh copper TEM grid (Ted Pella #01800), dried under N_2 gas and imaged with AFM or TEM, as described below.

2.2. Atomic force microscopy (AFM)

AFM was conducted with either a Digital Instruments Bioscope AFM with NanoScope IV controller or an Asylum Research MFP3D AFM. Both AFMs rest on inverted optical microscopes (Zeiss Axiovert 200M or Nikon 300TE), which allows accurate positioning of the tip over the sample. AFM began within 10–30 min of preparing the samples. Cantilevers included Olympus AC160TS and AC240TS tips (tip radii <10 nm) and silicon nitride probes from Bruker (DNP-10; tip radius of 20–60 nm).

AFM imaging was conducted in phosphate buffered saline (PBS), pH 7.4, or air with relative humidity ~40%, at room temperature. For protein experiments, 10 μg/mL of stock solution was spotted onto freshly cleaved mica or cleaned magnetite, incubated for 60 s, rinsed with PBS and imaged. For microorganism imaging, bacteria growing in liquid medium were spotted onto OTS-coated slides, incubated for 5 min, washed with PBS and then imaged (Yongsunthon and Lower, 2005). Images were recorded at a line frequency of <1 Hz and 512 × 512 pixels or 1024 × 1024 pixels. Scans of the mica or magnetite were 500 nm × 500 nm or less.

2.3. Transmission electron microscopy

Magnetotactic bacteria or magnetosomes were adsorbed to formvar stabilized and carbon coated 200 mesh copper grids (Ted Pella #01800). The grids were placed with the carbon side down on a drop of cell suspension or magnetosome suspension for 10 min, then immediately washed one time by placing the grid on a drop of water for 30 s. For staining, the grids were placed on a drop of 2% uranyl acetate (Ted Pella #19481) for either 30 s or 5 min, then dried completely using a piece of filter paper. The grids were analyzed using transmission electron microscopy using either an FEI Tecnai Spirit at 80 kV or with a FEI Tecnai F20 using high angle annular dark field STEM at 200 kV.

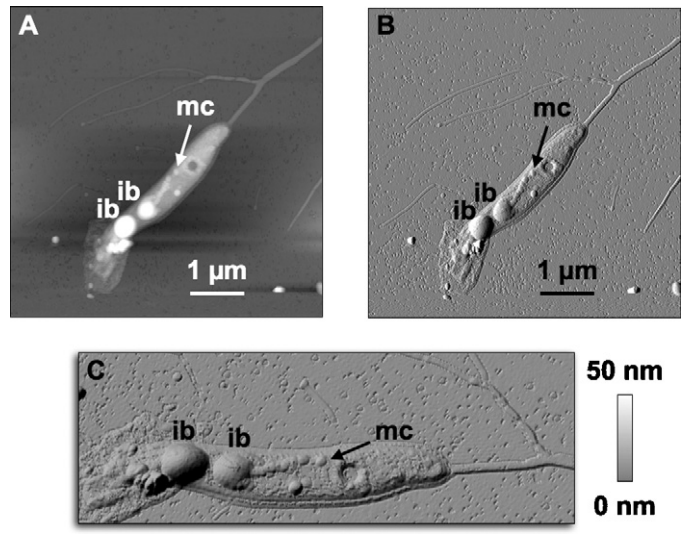

Fig. 1. (A) Topography and (B) amplitude images of *M. gryphiswaldense* MSR-1 acquired with tapping mode AFM. (C) Three-dimensional topography/amplitude composite image of *M. gryphiswaldense* MSR-1. Inclusion bodies (ib) and magnetosome chain (mc) are shown. Scale bars for length are provided inside each AFM image. A color-coded scale bar for height is provided to the right of (C).

3. Results

3.1. Imaging microorganisms, proteins, and antibodies with AFM

Fig. 1 shows a tapping-mode AFM image of *M. gryphiswaldense* MSR-1. Simultaneous height (Fig. 1A) and amplitude (Fig. 1B) images were collected on this sample. The height image shows the topography of the sample, that is, the lateral and vertical (z) dimensions of the cell. The amplitude image, on the other hand, is essentially a derivative of the height image, and therefore highlights edges or other features that may be hardly detectable in the height image. While the z information is lost, the appearances of features in an amplitude image (e.g., shape of bacterium) are similar to those seen with an optical or electron microscope.

Subcellular structures are visible in both the height and amplitude images shown in Fig. 1. Two intracellular inclusion bodies can be seen as bright white circles with a diameter of approximately 250 nm (Fig. 1A). The inclusions can also been seen in the amplitude image (Fig. 1B) as gray slightly irregular circles. Fig. 1 also shows a chain of approximately 8 magnetosomes running longitudinally down the center of the bacterium. The magnetosomes can be seen much more clearly in the amplitude image (Fig. 1B) and each magnetosome is approximately 75 nm in diameter. A single flagellum is located at the top polar end of the bacterium (Fig. 1). The thickness of the flagellum is approximately 100 nm, which is larger than expected but likely an artifact distorted by the edges of the AFM tip. It appears that the bottom polar end of the cell lysed open (Fig. 1), which could have been caused by the AFM tip as it was raster scanned across the cell surface during imaging. As a result, some of the bacterium's intracellular contents were released onto the TEM grid (Fig. 1).

3.2. AFM of Mms6 proteins synthesized by M. magneticum AMB-1

We also used AFM to collect images of purified Mms6 proteins on Fe_3O_4 (Fig. 2). Mms6 is a magnetosome-associated protein that is synthesized by *M. magneticum* AMB-1 and is believed to be involved in the biomineralization of Fe_3O_4 (Amemiya et al., 2007; Bazylinski and Frankel, 2004). A 100 μL drop of purified Mms6 (10 μg/mL) was spotted onto a cleaned Fe_3O_4 crystal and incubated for 10 min at

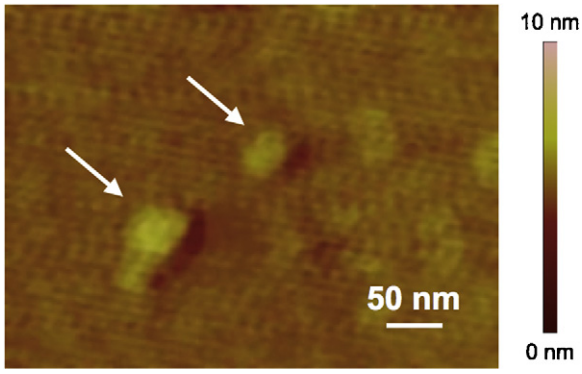

Fig. 2. Topography of Mms6 protein molecules deposited on magnetite (Fe_3O_4) and acquired with tapping mode AFM. Arrows indicate the position of Mms6 proteins. A scale bar for length is provided inside the figure. A color-coded scale bar for height is provided to the right of the topography image. (For interpretation of the references to color in this figure legend, the reader is referred to the web version of the article.)

room temperature. Next, the sample was gently washed with 1 mL of PBS and imaged by tapping mode AFM (Fig. 2). Fig. 2 shows the basic morphology that was observed for Mms6. All of the Mms6 proteins that were observed with AFM had the same oblong morphology and an approximate size of 25 nm × 50 nm (Fig. 2). The height of each Mms6 protein was approximately 7 nm (Fig. 2).

Since Mms6 had never before been imaged with AFM, we wanted to compare the morphology of Mms6 (Fig. 2) to protein structures, such as antibodies, that have been previously imaged by AFM. Therefore, we used AFM to collect images of purified green fluorescent protein (GFP) antibody molecules (Fig. 3). A 100 μL drop of 1:1000 anti-GFP (RDI Fitzgerald Inc.) diluted in PBS was spotted onto freshly cleaved mica. Mica was used in place of magnetite because the antibodies readily bind to mica. The antibodies were incubated for 10 min at room temperature, gently washed with 1 mL of PBS and imaged by tapping mode AFM.

Fig. 3 shows the three basic morphologies that were observed for the anti-GFP molecules. Some molecules appeared to have one domain (Fig. 3A) with a size of approximately 8 nm × 12 nm. Other molecules appeared to have a V-shaped morphology consisting of two domains with roughly equal dimensions (6 nm × 8 nm), which were connected to one another by a smaller 3 nm × 3 nm domain. Finally, a third Y-shaped morphology was observed on the mica. These structures consisted of three approximately equal oval-shaped domains. Each domain was roughly 6 nm × 8 nm. The height of all the antibodies observed in Fig. 3 appeared to be 4 nm. For comparison, the three-dimensional morphologies and sizes of antibodies, including their Fab and Fc fragments, are provided in Fig. 3 beside each topographic image (Silverton et al., 1977). The sizes and shapes of the antibodies observed in our topographic images (Fig. 3) are consistent with Silverton et al. (1977) and previously published images (Kienberger et al., 2004; San Paulo and Garcia, 2000).

3.3. TEM of *M. gryphiswaldense* MSR-1

Fig. 4 shows a single *M. gryphiswaldense* MSR-1 bacterium that was imaged by TEM. A single flagellum, approximately 8 μm long, can be seen attached to the bacterium (Fig. 4). Pieces of flagella <2 μm in length can also be seen in the TEM image of *M. gryphiswaldense* MSR-1 (Fig. 4). Despite great care in sample preparation, these pieces of flagella were likely sheared off during TEM sample preparation.

The TEM image (Fig. 4) also shows two intracellular inclusion bodies, which can be seen as light gray irregularly shaped circles. TEM also revealed two chains of approximately 20 magnetosomes

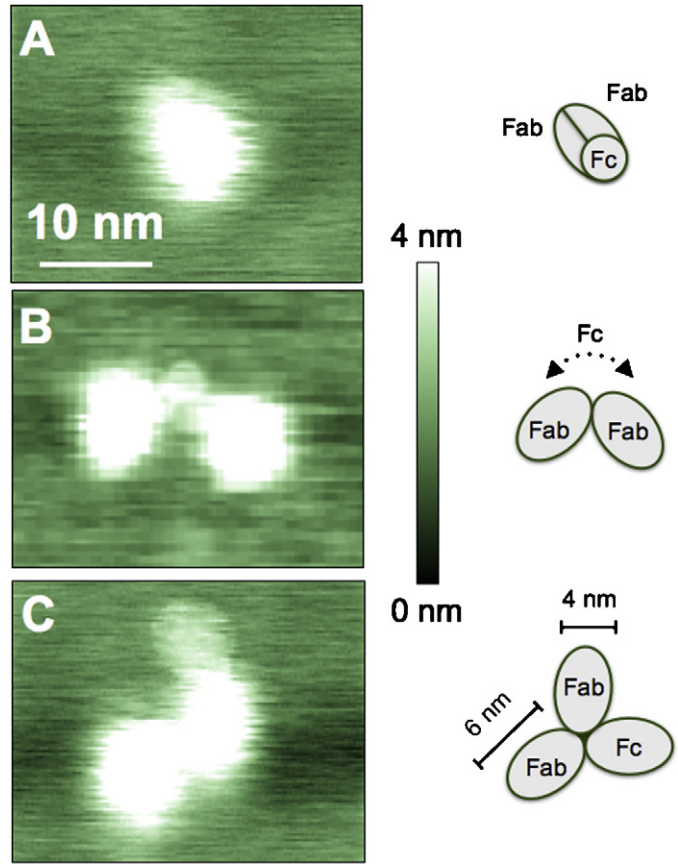

Fig. 3. Topography of anti-GFP molecules deposited on mica and acquired with tapping mode AFM. The anti-GFP molecules were observed to have (A) globular, (B) V-shaped, or (C) Y-shaped morphologies. The drawings to the right show the different conformations of the Fab and Fc fragments of the antibodies (Silverton et al., 1977). A scale bar for length is provided inside (A). A color-coded scale bar for height is provided to the right of the topography images. (For interpretation of the references to color in this figure legend, the reader is referred to the web version of the article.)

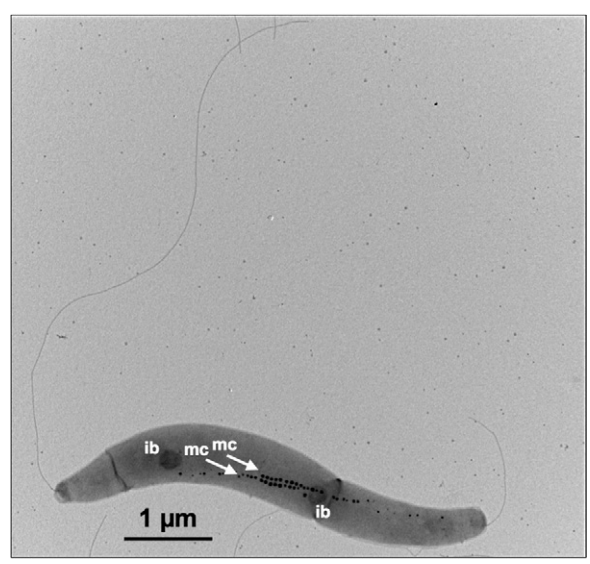

Fig. 4. TEM image of *M. gryphiswaldense* MSR-1. Inclusion bodies (ib) and two magnetosome chains (mc) are shown. A scale bar for length is provided.

(black particles) each running along the longitudinal axis of the *M. gryphiswaldense* MSR-1 bacterium (Fig. 4). These subcellular structures that were observed in the TEM image of Fig. 4 are similar to those seen in the AFM image of *M. gryphiswaldense* MSR-1 (Fig. 1).

3.4. AFM and TEM of magnetosomes produced by M. gryphiswaldense MSR-1

Magnetosomes were purified from *M. gryphiswaldense* MSR-1 using a previously described protocol (Grunberg et al., 2004) and imaged by both TEM and AFM (Fig. 5). The TEM image (Fig. 5A) shows nine cubo-octohedral magnetosomes arranged in a chain. The magnetosome membrane can been seen as a light-gray structure encasing dark-black/gray Fe_3O_4 crystals (Fig. 5A). The membrane can be clearly seen connecting several of the magnetosomes (e.g., the first and second magnetosome in Fig. 5A). The magnetosomes range in size from roughly 30 to 75 nm.

Fig. 5B shows a phase contrast image of a single magnetosome particle collected using AFM. The phase contrast image is shown here because it highlights nanometer-scale variations in the magnetosome particle that are not apparent in topography images. The magnetosome is approximately 120 nm in diameter (Fig. 5B), which is approximately twice a large as the magnetosomes imaged by TEM (Fig. 5A). The sides of the particle appear to adhere to the AFM tip more readily (bright white color along the perimeter of the particle) than the top of the particle (Fig. 5B). The top of the magnetosome (gray/black color) is similar to the substrate that the magnetosome is sitting upon (Fig. 5B). As expected, this suggests that there are variations in the material composition of the magnetosome (i.e., organic membrane surrounding an inorganic Fe_3O_4 crystal).

4. Discussion

Imaging live microorganisms with AFM can be a powerful tool to study biogeochemical processes in situ. Sample preparation is fairly simple because the only requirement for imaging is that the biological sample be adsorbed to a solid substrate (e.g., mica, magnetite), which can then be placed into the microscope. In Fig. 1 we demonstrated how tapping-mode AFM could be used to image live *M. gryphiswaldense* MSR-1 cells and subcellular structures such as inclusion bodies and magnetosomes. Inclusion bodies and magnetosomes are both intracellular structures, but we were still able to image them with AFM (Fig. 1) even though it is only capable of imaging surfaces. The reason we could image them here was because the inclusion bodies and magnetosomes pushed up against the inside of the bacterial membrane causing their structures to "show" through the cell membrane, which allowed us to image them with AFM.

TEM, on the other hand, is able to image intracellular structures. When TEM was used to image *M. gryphiswaldense* MSR-1 we observe inclusion bodies and two magnetosome chains (Fig. 4). The resolution of the TEM image (Fig. 4) is definitely better than that of the AFM image collected on *M. gryphiswaldense* MSR-1 (Fig. 1). However, we must remember that the TEM image of *M. gryphiswaldense* MSR-1 (Fig. 4) is of a bacterium that has been fixed on a TEM grid and so it is no longer alive when it is imaged. The *M. gryphiswaldense* MSR-1 bacterium that was imaged by AFM (Fig. 1) was not fixed prior to imaging and was presumably still alive when we imaged it with AFM. The microorganisms imaged by AFM (Fig. 1) and TEM (Fig. 4) provide complementary data about the subcellular structures (i.e., size, shape, location) that are synthesized by the microbe. While it would be possible, although difficult, to image the exact same microorganism we did not do this here because the bacteria were obtained from the same culture and so they should be essentially identical microorganisms.

Many smaller geobiological samples, such as the magnetosomes shown in Fig. 5, require scan sizes on the order of 500 nm × 500 nm. The resolution achieved by AFM (Fig. 5B) was comparable to the resolution achieved by TEM (Fig. 5A). The magnetosome membrane surrounding the Fe_3O_4 nanocrystals was visible by TEM (Fig. 5A). In the TEM image (Fig. 5A), the membrane appeared as a gray "sticky" substance between the black Fe_3O_4 nanocrystals. Very little membrane was observed surrounding the black Fe_3O_4 nanoparticles. However, in the AFM phase image of the magnetosome (Fig. 5B), it is clear that a "sticky" biological membrane (shown in white in Fig. 5B) surrounds the entire Fe_3O_4 nanocrystal. The size of the individual magnetosome imaged by AFM (Fig. 5B) is larger than the individual magnetosomes imaged by TEM (Fig. 5A). This difference is due to the fact that the AFM image (Fig. 5B) was collected under "physiological" conditions (i.e., PBS, pH 7.4), whereas the sample prepared for TEM was fixed, dried and imaged in vacuum (Fig. 5A). The AFM image (Fig. 5B) likely shows how the magnetosome, with its lipid bilayer coating, exists inside a living bacterium. It should be noted that the size and shape of the magnetosome observed by AFM (Fig. 5B) was similar to images published in a previous study that also used AFM to image magnetosomes isolated from a magnetotactic bacterium (Yamamoto et al., 2010).

Inside living magnetotactic bacteria, the magnetosomes exist as a chain (Bazylinski and Frankel, 2004). While we were able to successfully image an isolated magnetosome chain by TEM (Fig. 5A), despite multiple attempts, we were never able to locate and image a chain of magnetosomes by AFM. Therefore, the AFM image provided in Fig. 5B shows a single magnetosome. Nonetheless, Fig. 5 demonstrates that by combining AFM with TEM a more thorough characterization of the geobiological material is achievable. One method permits the visualization of the magnetosome chain, while the other method allows for the examination of the magnetosome's lipid bilayer.

In Fig. 2 we used AFM to image Mms6 protein molecules from *M. magneticum* AMB-1. The proteins were deposited onto a magnetite crystal and imaged with tapping-mode AFM. Magnetite was selected as the substrate because the proteins would readily bind to this mineral and because magnetite is the natural substrate for Mms6 in *M. magneticum* AMB-1. Mms6 proteins had an oblong-spherical shape with an approximate size of 25 nm × 50 nm and height of 7 nm (Fig. 2). Since this was the first time that a biomineralizing protein from a magnetotactic bacteria had been imaged by AFM, we wanted to compare its size and shape to a known protein. Anti-GFP was selected because it is a well-characterized protein that has a known structure, morphology and size (Kienberger et al., 2004; San Paulo and Garcia, 2000; Silverton et al., 1977).

Mms6 displayed one shape when imaged by AFM (Fig. 2), but anti-GFP molecules displayed three distinct morphologies (Fig. 3), each with an approximate size of 10–25 nm × 10–25 nm and height of 5 nm. While the heights of anti-GFP and Mms6 were comparable (i.e., 5 nm for anti-GFP; 7 nm for Mms6), the size of Mms6 was approximately twice as large as the anti-GFP molecules. This suggests that the Mms6 molecules aggregated together on the magnetite substrate such that the oblong-spherical shapes observed in Fig. 2 were actually >1 Mms6 molecule. These results were consistent with previous in vitro AFM studies of purified MamA proteins that formed oligomeric complexes on mica (Yamamoto et al., 2010). MamA is localized to the surface of the magnetosome membrane in *M. magneticum* AMB-1 and is believed to function in magnetosome chain assembly, activation and perhaps stabilization (Komeili et al., 2004; Yamamoto et al., 2010). Our results suggest that Mms6 behaves like MamA in vitro and exists as oligomer. We are currently purifying other Mms proteins from *M. magneticum* AMB-1 so that we can image them by AFM to determine if they also form protein–protein complexes on magnetite. Such information would

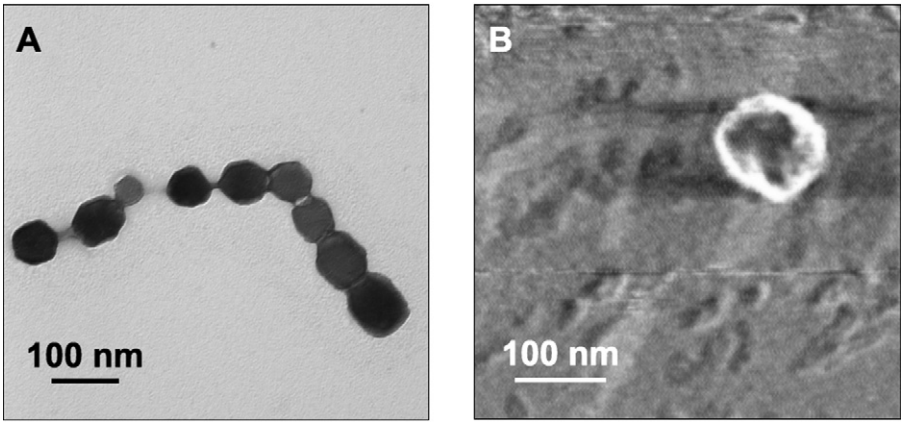

Fig. 5. (A) TEM image of magnetosomes and (B) AFM phase image of a magnetosome isolated from *M. gryphiswaldense* MSR-1. The AFM image was collected using tapping mode. Scale bars for length are provided for both images.

provide beneficial insight into possible protein–protein complexes that may be important in Fe_3O_4 biomineralization in vivo.

In addition to imaging, AFM can be used to perform nanoscale manipulations of biological samples. In Fig. 1 the AFM tips appears to have dissected the *M. gryphiswaldense* MSR-1 cell causing its internal cellular material to be released onto the substrate (Fig. 1). While the cellular lysis was accidental here, this example illustrates the utility of using AFM-assisted micro-dissection to extract and manipulate intracellular structures, such as magnetosomes or inclusion bodies, which may not be accessible to the AFM tip as it is raster scanned across the surface of a live microorganism. As such, the AFM cantilever could be used to perform microdissection on a live microorganism and subsequently image these intracellular structures by AFM. Yamamoto et al. (2010) actually demonstrated the utility of this technique when they used AFM-assisted microdissection to obtain images of magnetosomes adsorbed onto mica substrates (Yamamoto et al., 2010).

Acknowledgements

This work was supported by grants from the U.S. National Science Foundation (EAR-0920299, EAR-0920718, EAR-0745808). CJL wishes to thank project CGL2010-18274 from the Ministerio de Educación and grant GREIBBIO103 from Junta de Andalucía. We are grateful to D. Keene for providing the antibodies, and the editor and reviewers who provided insightful comments and suggestions.

References

Amemiya, Y., Arakaki, A., Staniland, S.S., Tanaka, T., Matsunaga, T., 2007. Controlled formation of magnetite crystal by partial oxidation of ferrous hydroxide in the presence of recombinant magnetotactic bacterial protein Mms6. Biomaterials 28, 5381–5389.

Barton, L.L., Fauque, G.D., 2009. Biochemistry physiology and biotechnology of sulfate-reducing bacteria. Advances in Applied Microbiology 68, 41–98.

Bazylinski, D.A., Frankel, R.B., 2004. Magnetosome formation in prokaryotes. Nature Reviews Microbiology 2, 217–230.

Dittrich, M., Luttge, A., 2008. Microorganisms, mineral surfaces, and aquatic environments: learning from the past for future progress. Geobiology 6, 201–213.

Edwards, K.J., Bach, W., McCollom, T.M., 2005. Geomicrobiology in oceanography: microbe–mineral interactions at and below the seafloor. Trends in Microbiology 13, 449–456.

Grunberg, K., Muller, E.C., Otto, A., Reszka, R., Linder, D., Kube, M., Reinhardt, R., Schuler, D., 2004. Biochemical and proteomic analysis of the magnetosome membrane in *Magnetospirillum gryphiswaldense*. Applied and Environmental Microbiology 70, 1040–1050.

Hernández-Hernández, A., Rodríguez-Navarro, A.B., Gómez-Morales, J., Jimenez-Lopez, C., Nys, Y., García-Ruiz, J.M., 2008. Influence of model globular proteins with different isoelectric points on the precipitation of calcium carbonate. Crystal Growth and Design 8, 1495–1502.

Heyen, U., Schuler, D., 2003. Growth and magnetosome formation by microaerophilic *Magnetospirillum* strains in an oxygen-controlled fermentor. Applied Microbiology and Biotechnology 61, 536–544.

Hochella Jr., M.F., Lower, S.K., Maurice, P.A., Penn, R.L., Sahai, N., Sparks, D.L., Twining, B.S., 2008. Nanominerals, mineral nanoparticles, and Earth systems. Science 319, 1631–1635.

Kienberger, F., Mueller, H., Pastushenko, V., Hinterdorfer, P., 2004. Following single antibody binding to purple membranes in real time. EMBO Reports 5, 579–583.

Komeili, A., Vali, H., Beveridge, T.J., Newman, D.K., 2004. Magnetosome vesicles are present before magnetite formation and MamA is required for their activation. Proceedings of the National Academy of Sciences of the United States of America 101, 3839–3844.

Madsen, E.L., 2011. Microorganisms and their roles in fundamental biogeochemical cycles. Current Opinion in Biotechnology 22, 456–464.

San Paulo, A., Garcia, R., 2000. High-resolution imaging of antibodies by tapping-mode atomic force microscopy: attractive and repulsive tip–sample interaction regimes. Biophysical Journal 78, 1599–1605.

Silverton, E.W., Navia, M.A., Davies, D.R., 1977. Three-dimensional structure of an intact human immunoglobulin. Proceedings of the National Academy of Sciences of the United States of America 74, 5140–5144.

Weber, K.A., Achenbach, L.A., Coates, J.D., 2006. Microorganisms pumping iron: anaerobic microbial iron oxidation and reduction. Nature Reviews Microbiology 4, 752–764.

Yamamoto, D., Taoka, A., Uchihashi, T., Sasaki, H., Watanabe, H., Ando, T., Fukumori, Y., 2010. Visualization and structural analysis of the bacterial magnetic organelle magnetosome using atomic force microscopy. Proceedings of the National Academy of Sciences of the United States of America 107, 9382–9387.

Yongsunthon, R., Lower, S.K., 2005. Force measurements between a bacterium and another surface in situ. Advances in Applied Microbiology 58, 97–124.